Dynamic Response Mechanisms of Stratified Rock Slopes Under Seismic Loading: Insights from Physical Modelling and Numerical Simulation

Fei Zhao
Department of Geotechnical Engineering, College of Civil Engineering, Tongji University, Shanghai 200092, China, zhaofei@tongji.edu.cn

Zhen_ming Shi
Key Laboratory of Geotechnical and Underground Engineering of the Ministry of Education, College of Civil Engineering, Tongji University, Shanghai 200092, China, 94026@tongji.edu.cn

Song_bo Yu
Key Laboratory of Geotechnical and Underground Engineering of the Ministry of Education, College of Civil Engineering, Tongji University, Shanghai 200092, China, yusongbo@tongji.edu.cn

ABSTRACT: In recent years, the construction of infrastructure projects, including roads, bridges, and tunnels, has given rise to severe engineering geological challenges. Particularly in alpine valley regions, seismic activities have triggered numerous geological hazards in stratified rock slopes. Notable examples include the 2008 Wenchuan Earthquake and the 2014 Ludian Earthquake, both of which caused substantial economic losses and human casualties. To investigate the dynamic response characteristics of rock slopes under seismic loading, this study carried out physical modeling tests and three-dimensional dynamic numerical simulations were conducted to systematically examine the dynamic response mechanisms of stratified rock slopes. The results indicate that the acceleration amplification within rock slopes under seismic excitation primarily exhibits three patterns: anomalous amplification at the interfaces of hard and soft rock layers, differential amplification associated with excitation directions, and coupled amplification induced by multi-directional seismic waves. Additionally, by analyzing the characteristics of Fourier spectrograms at different internal locations of the slopes, this study clarifies the dynamic response mechanisms of rock slopes under varying seismic intensities and excitation directions. These research outcomes hold significant engineering value for understanding the dynamic behavior of stratified rock slopes in seismic zones and guiding their reinforcement design.

1 INTRODUCTION

Under earthquake, the rock and soil mass of slopes is affected by strong seismic loads, leading to drastic changes in internal stress, which easily triggers geological hazards such as landslides and collapses (Wang et al., 2021; Goktepe and Coskun, 2025). Such hazards not only directly damage engineering facilities and block lifeline systems like transportation, water supply and power supply, but also may induce secondary disasters including debris flows and barrier lakes, posing a severe threat to the surrounding ecological environment as well as the lives and property of residents. For instance, the 2008 Wenchuan Earthquake triggered a lot of mountain landslides and collapses, forming numerous barrier lakes, which greatly increased the difficulty of emergency rescue and post-disaster reconstruction. Therefore, in-depth research on the dynamic response characteristics of slopes is crucial for revealing their failure mechanisms, accurately evaluating their stability, and formulating seismic reinforcement measures. It can not only ensure the seismic safety of projects and reduce the risk of secondary disasters, but also provide a scientific basis for project site selection, design and construction, helping to reduce economic losses and casualties. This is of great significance to the sustainable development of society.

The dynamic response of layered rock slopes is affected by multiple factors. Among them, the mechanical properties of rock and soil mass, such as elastic modulus, Poisson's ratio, internal friction angle, and cohesion, directly determine their deformation and failure characteristics. For instance, soft rock slopes are more prone to large deformation and failure during earthquakes compared to hard rock slopes (Feng et al., 2022; Liu et al., 2012). Geological structures like faults and joints weaken the integrity of rock mass, alter stress distribution, and increase the risk of instability. Meanwhile, regarding the geometric shape of slopes, the increase in slope height enhances the acceleration amplification effect at the slope upper, and the increase in slope angle reduces stability, and both factors are likely to induce sliding failure (Liu et al., 2021; Chen et al., 2024). In terms of seismic parameters, a larger wave amplitude leads to stronger inertial force and dynamic response of the slope; when the wave frequency is close to the natural vibration frequency of the slope, resonance is likely to occur, intensifying the response (Lin and Wang, 2006; Zhan et al., 2019); a longer duration results in greater cumulative damage to the slope and a higher probability of instability (Bouckovalas and Papadimitriou, 2005). At present, the action mechanisms of some factors still need in-depth research, especially the dynamic response laws and internal mechanisms of soft rock slopes under multi-directional seismic loads (Fu et al., 2015; Jiang et al., 2018).

Based on the above background and current research status, this study systematically explores the dynamic response mechanism of layered rock slopes by integrating methods such as on-site seismic monitoring, physical modeling tests, and three-dimensional dynamic numerical simulation. The research results hold significant engineering value for understanding the dynamic behavior of layered rock slopes in seismic zones and guiding their reinforcement design.

2 GEOLOGICAL BACKGROUND

The Shaba Slope is located in Ludian County, Yunnan Province, China, with a geographical coordinate of approximately 103°27′40″ E (East Longitude) and 27°09′08″ N (North Latitude). Field geological survey results show that the Shaba Slope is a typical bedding rock slope of alternating hard and soft layers. Its lithological composition is mainly composed of mudstone, muddy siltstone, and siltstone, which are distributed in an interbedded manner, with a rock stratum dip angle of 30°–35°. Among them, the mudstone and muddy siltstone are severely weathered. The physical and mechanical parameters of mudstone, muddy siltstone, and siltstone are obtained through laboratory geotechnical tests, as shown in Table 1.

Table 1. Physical and mechanical properties of rock mass in Shaba slope

Physical indicators	Physical symbols	Lithological composition		
		Siltstone	Muddy siltstone	Mudstone
Density	ρ (g/cm^3)	2.45-2.64	2.45-2.64	2.03-2.15
Tensile strength	τ (MPa)	4.50-6.30	4.50-6.30	/
Compressive strength	σ_c (MPa)	15-22	15-22	0.50-3.50
Elastic modulus	E (GPa)	4-6	4-6	0.38-2.1
Poisson's ratio	μ	0.20-0.23	0.20-0.23	0.25-0.35
Cohesion	c (MPa)	3-5	3-5	0.10-0.27
Internal friction angle	φ (°)	31-45	31-45	15-27

3 METHODOLOGY

3.1 Modelling test

In this study, geometric dimension L, density ρ, and acceleration a are selected as the main controlling physical quantities, and the similarity constant w (model/prototype) for each physical quantity is derived. Among them, the similarity constant for geometric dimension L is 1/16, while the similarity constants for density ρ and acceleration a are both 1. Based on the three similarity laws and the dimensional analysis method, the similarity relationships of the test model are designed, and the similarity constants for physical quantities related to material properties and dynamic performance are further derived. Subsequently, in accordance with the similarity design relationships, a series of proportioning experiments on rock mass similar materials are conducted in this study. Through a series of laboratory geotechnical engineering tests, the corresponding physical and mechanical parameters of the rock mass similar materials are finally determined, as shown in Table 2.

Table 2. Physical and mechanical indicators of model materials of rock slope

Rock Indicators	Density	UCS	Elastic modulus	Poisson's ratio	Cohesion	Internal friction angle	TS
	ρ (g·cm^{-3})	σ_c (MPa)	E (GPa)	μ	c (kPa)	φ (°)	σ_t (MPa)
Bedrock/Hard rock	2.47	2.21	0.37	0.22	0.47	31	0.20
Soft rock/Layer	2.07	0.19	0.004	0.33	0.013	22	0.01

Finally, after simplifying the prototype slope, a bedding rock slope model with alternating hard and soft layers is constructed in this study based on the similarity relationships, with dimensions of 3000 mm (length) × 1300 mm (width) × 1700 mm (height). Among the layers of the model, the thickness of the soft rock layer is 55 mm, and that of the hard rock layer is 110 mm. The slope model is built by combining masonry and casting methods: the bedrock part was constructed by masonry, while the hard rock and soft rock layers are formed by casting, as shown in Figure 1. A reinforcement form of a combined pile-anchor structure is also adopted in the slope model. In the test, acceleration sensors are arranged at 9 positions: P1–P7 from the bottom of the model to the slope upper, and P7–P9 from the upper to the lower of the slope surface. The seismic wave used for excitation in the test is the Ludian wave (Ms 6.8) recorded during the 2014 earthquake in Ludian County, Yunnan Province. The excitation direction was the X-direction, and the peak ground acceleration (PGA) ranged from 0.05g, 0.10g, 0.15g to 0.20g.

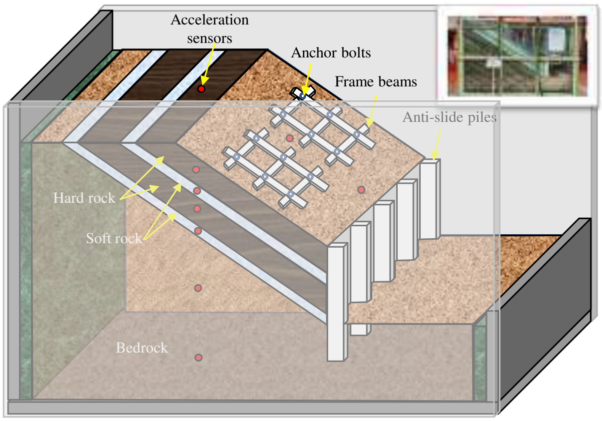

Figure 1. Schematic diagram of sensor and monitoring layout in model test

3.2 Numerical simulation

Based on the slope model used in the physical test, a numerical slope model reinforced with a combined pile-anchor structure is established using the finite difference method (FLAC3D). The slope has a length of 48 m, a width of 20.8 m, and a height of 27.2 m, as shown in Figure 5. The model consists of five parts: two hard rock layers, two soft rock layers, and a bedrock layer. Among them, each hard rock layer is approximately 1.76 m thick, and each soft rock layer is approximately 0.88 m thick. The Mohr-Coulomb constitutive model is adopted for the hard rock, soft rock, and bedrock. To reduce the reflection of seismic waves at the model boundaries, a quiet boundary is set at the bottom of the model, and free-field boundaries are set around the model. The Ludian wave is input vertically from the bottom of the model in the form of a stress time history, with intensities ranging from 0.05g to 0.20g. The excitation directions include four types: X, XY, XZ, and XYZ. For the calculation damping, a local damping coefficient of 0.1571 is used.

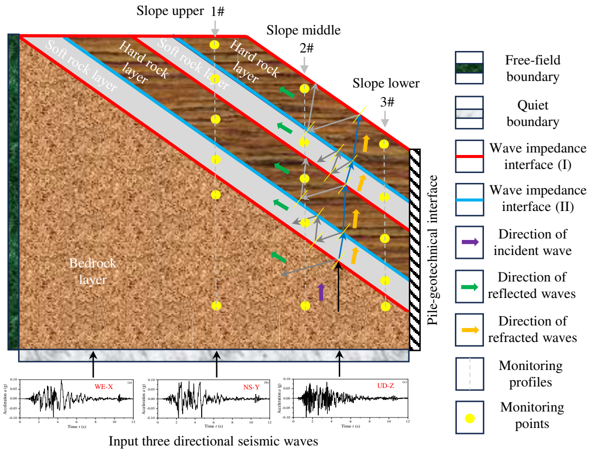

Figure 2. Ludian wave (WE, NS, UD): (a) Acceleration – time curve; and (b) amplitude – frequency curve

4 RESULTS AND DISCUSSION

Table 3 shows the distribution characteristics of peak accelerations at measuring points P1–P9 of the rock slope under X-direction excitation. The peak acceleration shows an increasing trend as the input seismic intensity increases, which is specifically manifested as follows: along the vertical upward direction inside the slope (P1–P7), the average peak acceleration at P1 (slope bottom) is 0.253g, while the peak acceleration at P6 (slope upper) increases to 0.397g. Along the upward direction of the slope surface (P9, P8, P7), the peak acceleration also shows an overall upward trend, and the average peak acceleration at P9 (slope lower) is 0.253g, and it rises to 0.368g at P8 (middle of the slope surface).

To compare the acceleration amplification law of the rock slope, this study takes P1 (the monitoring point at the slope bottom) as a reference to calculate the average acceleration amplification factors of monitoring points P2–P9 inside the slope. Analysis shows that under seismic wave excitation, the acceleration amplification factors of the slope along the internal vertical direction (P1–P7) and the upward direction of the slope surface (P9, P8, P7) generally show an upward trend. It can be seen from this that there is an obvious acceleration amplification effect when seismic energy is transmitted along the vertical direction inside the slope and the inclined upward direction of the slope surface. In addition, the acceleration amplification factor (AAF) also shows an obvious "differential amplification effect between hard and soft rock layers". Specifically, the AAF of soft rock is significantly higher than that of hard rock. For example, the average AAF values of the measuring points corresponding to the two soft rock layers inside the slope are 1.765 and 1.798 respectively, while the AAF values of the measuring points corresponding to the two hard rock layers are 1.728 and 1.766 respectively. This indicates that the amplification effect of soft rock on ground motion is 2.1% to 1.8% higher than that of hard rock.

Table 3. Peak acceleration and acceleration amplification factor of P1-P9 under X-direction excitation in modelling test

Monitoring point	PA (g)				AAF			
	0.05g	**0.10g**	**0.15g**	**0.20g**	**0.05g**	**0.10g**	**0.15g**	**0.20g**
P 1	0.049	0.126	0.144	0.199	1.000	1.000	1.000	1.000
P 2	0.101	0.153	0.207	0.325	2.061	1.214	1.438	1.633
P 3	0.116	0.189	0.230	0.354	2.367	1.500	1.597	1.779
P 4	0.115	0.187	0.230	0.341	2.347	1.484	1.597	1.714
P 5	0.118	0.196	0.240	0.356	2.408	1.556	1.667	1.789
P 6	0.117	0.192	0.237	0.348	2.388	1.524	1.646	1.749
P 7	0.128	0.214	0.251	0.358	2.612	1.698	1.743	1.799
P 8	0.115	0.190	0.232	0.349	2.347	1.508	1.611	1.754
P 9	0.050	0.107	0.135	0.215	1.020	0.849	0.938	1.080

Meanwhile, to further obtain the acceleration response laws of the slope surface and the interior of the slope, the numerical simulation is analyzed. By comparing its laws with those of the physical model test, they show the same variation trend, which verifies the validity of the numerical calculation results. Table 4 presents the acceleration amplification factors of different monitoring profiles of the slope under X-direction excitation, and the average acceleration amplification factors are obtained through calculation (see Figure 3(a)). It can be seen from the figure that under X-direction excitation, the slope exhibits an obvious elevation-dependent acceleration amplification effect, whether in the interior or on the surface of the slope. Moreover, there is a significant differential amplification phenomenon in rock layers with different strengths. The differential acceleration amplification effect of different rock layers under ground motion is essentially the result dominated by the difference in rock mass stiffness, coupled with the combined action of material damping characteristics and the complex wave effects of seismic waves generated at interlayer interfaces. Specifically, due to its low inherent stiffness, the soft rock layer has weak impedance to the input ground motion, which allows vibration energy to be more easily input and accumulated within the layer. Meanwhile, soft rock usually has high damping characteristics that can dissipate part of the energy; however, its overall response is still dominated by significant displacement and acceleration amplification. In addition, seismic waves undergo reflection, refraction, and scattering at the interface between soft and hard rock layers, leading to the generation and superposition of interface waves (such as Love waves and Rayleigh waves). This further enhances the vibration response of the soft rock layer, making it a "sensitive area" for acceleration amplification (see Figure 2). In contrast, hard rock layers exhibit strong constraint on seismic wave propagation due to their high stiffness and strength, so vibration energy is not easy to accumulate. Moreover, their low damping characteristics enable energy to diffuse outward and attenuate rapidly, resulting in a relatively weak acceleration amplification effect.

Taking the seismic wave intensity with PGA=0.10g as an example, spectral analysis of bedrock, soft rock, and hard rock supports the above view (see Figure 4). As shown in Figure 4(a), when seismic waves propagate from bedrock (A1-2#) to soft rock (A2-2#), amplification of fixed frequency bands increases significantly (with multiple peak amplitudes P1-P4)—the first sensitive frequency band expands to 0-25 Hz and a new one (40-80 Hz) appears; when waves move from soft rock (A2-2#) to hard rock (A3-2#), the first sensitive frequency band further expands to 0-30 Hz, while the second shrinks to 40-60 Hz and its peak drops from 0.120 m/s² to 0.042 m/s². This is because soft-hard interlayered slopes are sensitive to specific seismic frequency bands, and soft rock's higher sensitivity than hard rock enhances amplification; increasing soft rock thickness and quantity can further intensify its vibration, risking severe slope failure. Meanwhile, Figure 4(b) shows that from slope foot (A2-3#) to top (A2-1#), the sensitive frequency bands (in length and peak) at the middle (A2-2#) and top are significantly larger than those at the foot: the first sensitive frequency bands are 0-18 Hz (A2-1#), 0-25 Hz (A2-2#), 0-31 Hz (A2-3#) with peaks 0.395, 0.406, 0.407 m/s² respectively, and the second are 53-65 Hz (A2-1#), 40-80 Hz (A2-2#), 60-80 Hz (A2-3#) with peaks 0.057, 0.120, 0.068 m/s² respectively. This confirms that seismic wave field superposition is most significant in the upper slope, resulting in the strongest seismic response.

Table 4. Acceleration amplification factors of different monitoring profiles of slope under X-direction excitation in numerical simulation

Monitoring profiles	Monitoring points	PGA				Average value
		0.05g	0.10g	0.15g	0.20g	
Slope upper (profile 1#)	A1	1.17	1.13	1.06	1.17	1.13
	A2	1.58	2.02	1.13	1.59	1.58
	A3	1.73	1.56	1.54	1.77	1.65
	A4	1.76	1.65	1.93	1.87	1.80
	A5	1.79	1.85	1.63	1.67	1.74
Slope middle (profile 2#)	A1	1.13	1.04	1.17	1.12	1.12
	A2	1.70	1.11	1.56	1.41	1.45
	A3	1.55	1.56	1.77	1.67	1.64
	A4	1.76	1.72	2.22	1.61	1.83
	A5	1.72	1.58	1.56	1.71	1.64
Slope lower (profile 3#)	A1	1.03	1.16	1.11	1.04	1.09
	A2	1.08	1.29	1.26	1.09	1.18
	A3	1.48	1.88	1.31	1.44	1.53
	A4	1.55	1.78	1.58	1.60	1.63
	A5	1.52	1.58	1.67	1.65	1.61

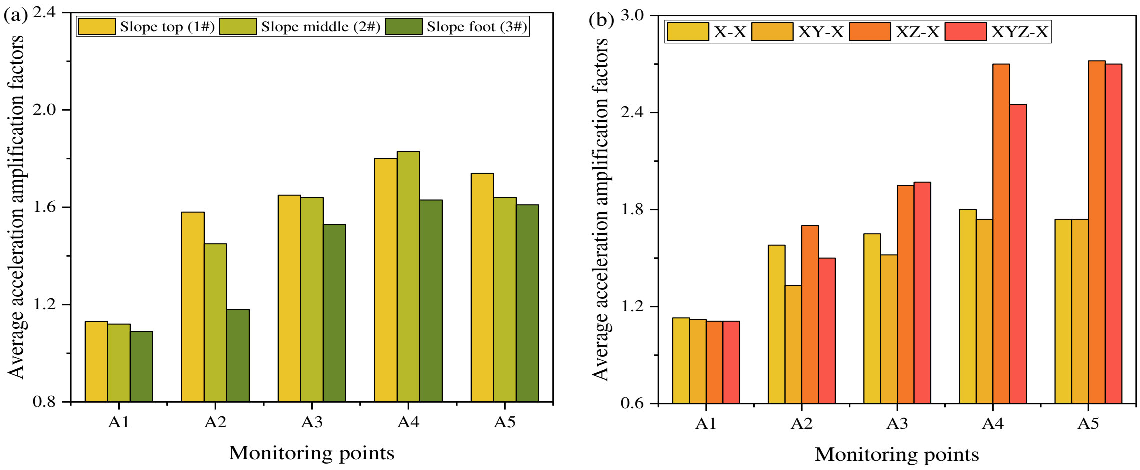

Figure 3. Average acceleration amplification factors of different monitoring profiles of slope under different excitation directions in numerical simulation: (a) Different monitoring profiles; and (b) different excitation directions

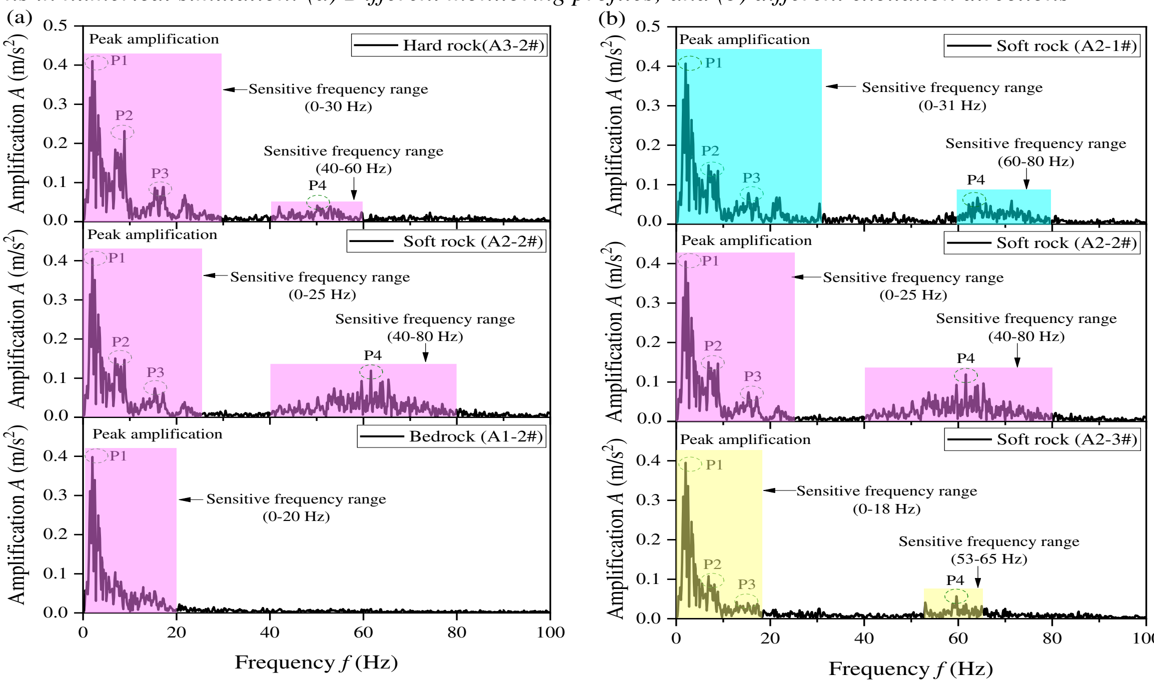

Figure 4. Amplification- frequency curves of rock slopes: (a) Different rock layers, and (b) different monitoring points

Table 5 presents the acceleration amplification factors of the slope in the X-direction under different excitation directions, and the average acceleration amplification factors are obtained through calculation (see Figure 3(b)). It can be seen from the figure that under the four excitation directions (X, XY, XZ, and XYZ), the slope exhibits an acceleration coupling amplification phenomenon. Specifically, compared with X-direction excitation, this coupling effect is reflected in the fact that under the XY, XZ, and XYZ excitation directions, the slope has the strongest dynamic response in the XZ direction and the weakest in the XY direction. The order of dynamic response intensity from strongest to weakest is XZ, XYZ, X, and XY. This indicates that the addition of Y-direction seismic waves weakens the seismic response, while the addition of Z-direction seismic waves significantly enhances the seismic response. Comprehensive analysis shows that the main reasons for the above phenomenon are as follows: the introduction of Y-direction seismic waves causes an "energy competition" or "phase cancellation" effect with X-direction vibration, thereby inhibiting the amplification of X-direction acceleration; in contrast, Z-direction vibration changes the normal stress state inside the slope, reduces the shear stiffness of the slope, and makes it easier for the vibration energy in the X-direction to be transmitted and amplified. Ultimately, this leads to the coupled enhancement of the X-direction dynamic response.

Table 5. Acceleration amplification factors of X-direction of slope under different excitation directions in numerical simulation

Excitation direction	Monitoring point	PGA				Average value
		0.05g	0.10g	0.15g	0.20g	
XY-X	A1	1.15	1.14	1.03	1.17	1.12
	A2	1.38	1.44	1.16	1.35	1.33
	A3	1.60	1.45	1.45	1.59	1.52
	A4	1.67	1.96	1.74	1.60	1.74
	A5	1.72	1.87	1.71	1.66	1.74
XZ-X	A1	1.15	1.07	1.06	1.14	1.11
	A2	1.63	2.03	1.29	1.85	1.70
	A3	1.99	1.93	1.79	2.08	1.95
	A4	2.46	2.46	3.13	2.74	2.70
	A5	2.78	2.51	2.92	2.67	2.72
XYZ-X	A1	1.14	1.09	1.04	1.15	1.11
	A2	1.54	1.84	1.12	1.48	1.50
	A3	1.87	2.21	1.93	1.87	1.97
	A4	2.56	2.52	2.25	2.47	2.45
	A5	2.58	3.04	2.44	2.72	2.70

5 CONCLUSIONS

1) Peak acceleration increases with input intensity and elevation: Under X-direction excitation, the peak acceleration at each slope monitoring point rises with input ground motion intensity (0.05g–0.20g). It also increases vertically upward inside the slope (P1→P6: 0.253g→0.397g) and upward along the slope surface (P9→P8: 0.253g→0.368g), showing a distinct elevation effect.

2) Acceleration amplification: spatial consistency & lithological differences: Acceleration Amplification Factors (AAF) show an overall upward trend both vertically inside the slope and upward along the surface. Soft rock has higher average AAF (1.765, 1.798) than hard rock (1.728, 1.766), with a 1.8%–2.1% stronger amplification effect. Dominated by rock stiffness differences and interlayer wave superposition, soft rock acts as an amplification "sensitive zone".

3) Multi-directional excitation: coupled amplification & significant directional impact: Under multi-directional (XY, XZ, XYZ) excitation, the slope shows X-direction coupled amplification, with dynamic response intensity in the order: XZ > XYZ > X > XY. Y-direction waves weaken X-response, while Z-direction waves enhance it by altering slope stress and reducing shear stiffness.

ACKNOWLEDGEMENTS

This research is supported by the China Postdoctoral Science Foundation (Grant No. 2025M770468), and National Key Research and Development Program of China (Grant No. 2023YFC3008300 and 2019YFC1509700).

REFERENCES

Feng, J. Zhang, Y.B. He, J.X. et al. (2022). Dynamic response and failure evolution of low-angled interbedding soft and hard stratum rock slope under earthquake. *Bulletin of Engineering Geology and the Environment*, 81(10):400.

Liu, H.X. Qiu, T. Xu, Q. (2021). Dynamic acceleration response of a rock slope with a horizontal weak interlayer in shaking table tests. *PLoS ONE*, 16(4): e0250418.

Liu, H.X. Xu, Q. Zou, W. et al. (2012). Shaking table test study on the vertical seismic behavior for the layered rock slopes. *Journal of Vibration and Shock,* 31:13–19+28.

Chen, G.P. Yang, C.W. Qu, L.M. et al. (2024). Shaking table test and numerical analysis of dynamic response and damage mechanism of a deposit slope with a weak interlayer reinforced by a pile–anchor structure. *Structures*, 59: 105728.

Lin, M.L. and Wang, K.L. (2006). Seismic slope behavior in a large-scale shaking table model test. *Engineering Geology*, 86(2): 118-133.

Zhan, Z.F. Qi, S.W. He, N.W. et al. (2019). Shaking table test study of homogeneous rock slope model under strong earthquake. *Journal of Engineering Geology*, 27(5): 946-954. DOI: 10.13544/j.cnki.jeg.2019168

Bouckovalas, G.D. Papadimitriou, A.G. (2005). Numerical evaluation of slope topography effects on seismic ground motion. Soil Dynamics and Earthquake Engineering, 2005, 25, 547–558

Fu, X. Fan, G. Liu, F.C. et al. (2015). Shaking table tests on the acceleration response of anti-dip stratified rock slope with composite retaining structure. *China Earthquake Engineering Journal,* 37, 823–828.

Jiang, X.L. Niu, J.Y. Yang, H. et al. (2018). Large-scale shaking table model test study of seismic response characteristics on layered rock slope with tunnel. *Chinese Journal of Applied Mechanics*, 35: 762–768.

Goktepe, F., Coskun, K. (2025). Analysis of seismic ground response and soil-structure interaction on step-like topography due to rock-outcrop motions. *Soil Dynamics and Earthquake Engineering*, 188: Part A.

Wang, C.Y. Liu, X. Song, D. et al. (2021). Numerical investigation on dynamic response and failure modes of rock slopes with weak interlayers using continuum-discontinuum element method. *Frontiers in Earth Science*, 9(9):791458.